IEEE Access
Multidisciplinary | Rapid Review | Open Access Journal

SPECIAL SECTION ON NEW WAVEFORM DESIGN AND AIR-INTERFACE FOR FUTURE HETEROGENEOUS NETWORK TOWARDS 5G

Received July 17, 2019, accepted August 5, 2019, date of publication August 13, 2019, date of current version August 28, 2019.

Digital Object Identifier 10.1109/ACCESS.2019.2935038

Near Optimal Timing and Frequency Offset Estimation for 5G Integrated LEO Satellite Communication System

WENJIN WANG[1], (Member, IEEE), YUSHAN TONG[1,2], LINGXUAN LI[1], AN-AN LU[1], (Member, IEEE), LI YOU[1], (Member, IEEE), AND XIQI GAO[1], (Fellow, IEEE)

[1]National Mobile Communications Research Laboratory, Southeast University, Nanjing 210096, China
[2]Huawei Technologies Co., Ltd., Shanghai, China

Corresponding author: Wenjin Wang (wangwj@seu.edu.cn)

This work was supported in part by the National Key Research and Development Program of China under Grant 2018YFB1801103, in part by the National Natural Science Foundation of China under Grant 61761136016, Grant 61801114, Grant 61631018, Grant 61771264, Grant 61871465, and Grant 61501113, in part by the Civil Aerospace Technologies Research Project under Grant D010109, in part by the Natural Science Foundation of Jiangsu Province under Grant BK20170688, in part by the Fundamental Research Funds for the Central Universities, and in part by the Huawei Cooperation Project.

ABSTRACT The integration of satellite and terrestrial 5G networks aims to provide ubiquitous coverage, improve service reliability, and enable the network scalability. However, the inherent characteristics of satellite channels bring challenges on the air interface design of integrated terrestrial-satellite networks. For example, for low earth orbits (LEO) mobile satellite communication (SatCom) system, it is unclear so far whether the 5G new radio (5G-NR) synchronization signals could meet the requirement of timing and frequency offset estimation in the presence of large Doppler shifts. In this paper, we investigate time and frequency synchronization for the downlink transmission of 5G-NR signals over LEO satellite channels. Starting from the maximum log-likelihood criterion for timing offset estimation given the observation of the received primary synchronization signals (PSS), we derive an upper bound of the objective function for simplicity. With *a priori* information that the maximum Doppler shift of LEO satellite-ground link is within a specific range, we construct the local synchronization sequence via using the modulated discrete prolate spheroidal sequences (DPSS) vectors. Then the timing offset estimation can be recast into a one-dimensional peak search problem. Moreover, the cyclic prefix (CP) structure of orthogonal frequency division multiplexing (OFDM) can be utilized to improve the estimation performance further. Once the timing and frequency offset are captured in the above initial synchronization phase, the tracking synchronization can be much simplified as the variation of both the timing and frequency offset is very small between two adjacent synchronization blocks. Simulation results show that by using the proposed algorithms, the 5G-NR signals can achieve near optimal downlink time and frequency synchronization in typical LEO SatCom systems.

INDEX TERMS LEO satellite, 5G integrated network, time and frequency synchronization, Doppler shift.

I. INTRODUCTION

An integrated satellite-terrestrial communications network can take the advantages of both the satellite and the land mobile communications and thus can provide genuine ubiquitous coverage [1]–[4]. As the land mobile communications networks come into the 5G era, there has recently been a considerable research effort on defining an integration architecture of satellite communication (SatCom) and 5G networks [5]–[8]. In particular, aiming to foster the roll out of 5G service in un-served areas, reinforce the 5G service reliability, and to enable the scalability of 5G networks, the 3rd generation partnership project (3GPP) has been actively launched an study item on supporting non terrestrial networks with 5G New Radio (NR) [9]. In such integrated satellite-terrestrial networks, a major challenge to

The associate editor coordinating the review of this article and approving it for publication was Qilian Liang.

the user equipment (UE) is the requirement of exploiting both satellite and terrestrial links. Consequently, the air interface design of the satellite component should maximize utilization of the technology commonalities with the terrestrial systems, so as to reduce the implementation costs and simplify the interactive procedures.

As the basic waveform of 5G NR, the orthogonal frequency division multiplexing (OFDM) may suffer from the large carrier frequency offset (CFO) that destroys the orthogonality among all subcarriers and results in severe intercarrier interference (ICI) and intersymbol interference (ISI) [10], [11]. Meanwhile, the downlink timing synchronization of UE, which serves as the first stage to establish a communication link with the base station, will directly determine the performance of initial cell search in 5G networks [12]. The 5G NR synchronization signals have therefore been designed primarily for the ground wireless environments to acquire the timing and frequency offsets. However, in low earth orbits (LEO) satellites based mobile communication environments, the high-speed relative motion between the satellite and the UE generates a large Doppler frequency shift, sometimes greater than a couple of subcarrier spacing [13], [14]. Such significant differences between the satellite-to-ground channel and the ground wireless channel raise a question: *how to achieve accurate timing and frequency synchronization in the satellite-to-ground channel only with 5G NR synchronization signal?* This paper will try to provide an answer.

The timing and frequency offset estimation for OFDM transmission that have been investigated and developed over the past decades can be classified into three categories, namely the auto-correlation based estimation algorithms [15]–[24], the cross-correlation based estimation algorithms [25]–[29], and a combination thereof [30], [31]. The auto-correlation based estimation algorithms usually exploit the cyclic prefix (CP) structure of OFDM transmission to recover the timing and carrier frequency offset [19]–[24]. As the CP is added in a symbol by symbol manner, these algorithms are suitable for the scenarios where only the fractional frequency offset exists, i.e., the case where the CFO is less than one subcarrier spacing. For the cases where the CFO is larger than a couple of subcarriers, custom-designed synchronization signals with the repetition structure in the time domain are proposed for time and frequency synchronization [15]–[18]. In current terrestrial cellular communication systems, e.g., long term evolution (LTE) and 5G NR, the cross-correlation based estimation algorithms are used in the downlink timing and CFO estimation, with the help of specifically defined primary synchronization signals (PSS) [26]–[29]. However, these existing algorithms are designed particularly for the ground wireless channels with relatively low mobility, and their performance may degrade in the presence of large CFO in LEO satellite-to-ground links. To the best of our knowledge, little efforts have been put on the investigation of the downlink timing and CFO estimation algorithms in satellite-to-ground wireless channels with only the PSS of terrestrial cellular communication systems. This is the motivation for our work.

In the LEO communication system, Doppler frequency shift varies continuously between the maximum and the minimum value during a short period namely the visibility window, which is an only period that the satellite is visible to a ground UE [13]. It is therefore necessary to develop an accurate and fast synchronization algorithm in LEO scenario where large CFO exists. In this paper, we investigate the time and frequency synchronization in the downlink transmission and propose the timing and frequency offset estimation methods for the 5G integrated LEO mobile SatCom system. The major contributions of this paper are summarized as follows.

- Starting from the maximum log-likelihood criterion for timing offset estimation given the observation of the received PSS, we developed an upper bound of the objective function to allow a solvable optimization problem. For initial timing and frequency synchronization, the timing offset estimation is recast into a single variable optimization based on the fact that the Doppler frequency shift is limited and varies continuously during the visibility window.
- The modulated prolate spheroidal sequences (DPSS) are employed to develop a compatible implementation architecture of timing and frequency synchronization with conventional cross-correlation methods. The proposed method shows robust performance in the presence of a large Doppler frequency shift.
- We utilize the inherent CP structure of OFDM as auxiliary information to improve the performance of timing and frequency offset estimation. Meanwhile, with estimating a fractional frequency offset by the CP structure, the computational complexity of CFO estimation is further reduced.
- Based on the property that the Doppler shift and timing offset vary slightly between successive synchronization blocks in LEO satellite-to-ground channels, the computational complexity of timing and frequency offset estimation are simplified in the tracking synchronization phase.

The rest of this paper is organized as follows. Section II introduces a typical architecture of 5G integrated LEO SatCom and the time and frequency synchronization issue. Section III presents the proposed time and frequency synchronization algorithms in initial synchronization. Section IV presents the proposed timing and frequency offset estimation algorithm in tracking synchronization. Simulations are contained in Section V. Finally, the conclusion is drawn in Section VI.

We use the following notation throughout the paper: $\bar{\jmath} = \sqrt{-1}$ denotes the imaginary unit. $\mathbf{I}_N$ denotes the identity matrix of order N. Upper case boldface letters and lower case boldface letters are used for matrices and column vectors, respectively. The superscripts $(\cdot)^H$, $(\cdot)^T$, $(\cdot)^{-1}$ and $(\cdot)^*$ denote the conjugated-transpose, transpose, inverse and conjugate

operations, respectively. We employ $[\mathbf{a}]_i$ and $[\mathbf{A}]_{ij}$ to denote the i-th element of the vector $\mathbf{a}$, and the (i,j)-th element of the matrix $\mathbf{A}$, respectively. The notation $\mathrm{Re}\{\cdot\}$ stands for the real part of a complex-valued quantity, and $\arg(\cdot)$ denotes the phase of its argument. The notation $\mathrm{E}\{\cdot\}$ denotes the mathematical expectation operator. We use $\mathbf{a} \odot \mathbf{b}$ to denote the Hadamard product of two vectors $\mathbf{a}$ and $\mathbf{b}$ of the same dimensions and use $\langle\cdot\rangle_N$ to denote the modulo-N operation. Finally, all estimated parameters are described as $\hat{(\cdot)}$.

II. SYSTEM MODEL

A. 5G INTEGRATED LEO SATCOM

An essential feature of the 5G integrated LEO SatCom system is the ability to provide seamless service for 5G UE while roaming between the terrestrial and the satellite backhauled cells. Hence a key requirement for UE is the flexibility to support satellite and terrestrial dual-mode communication, as shown in Fig.1.

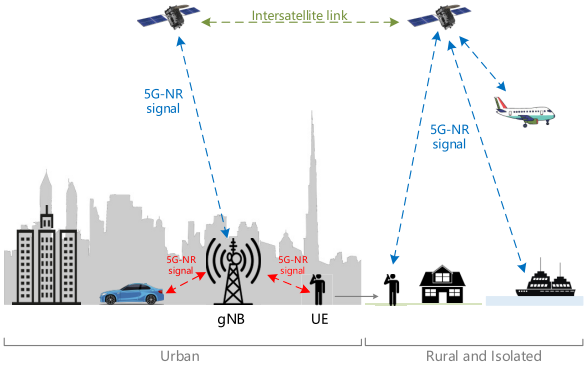

FIGURE 1. 5G Integrated LEO SatCom architecture.

For such an architecture, when UE is located in a high-density deployment of small cells like urban areas, the communication is largely based on the terrestrial link, while LEO satellite solutions can provide additional capacity for supplementation. In the rural and isolated regions outside the coverage areas of the terrestrial cellular communication system, LEO satellite links are able to deliver reliable connectivity to support the expansion of 5G systems. It should be noted that both terrestrial and satellite access links are expected to be implemented by 5G-NR air interface and thus no additional network infrastructure, as well as separately interactive procedures design, are required. This shows that the integration of the air interface design between the terrestrial and the satellite links can significantly bring down the deployment cost and implementation complexity of an integrated satellite-terrestrial network.

B. VARIATION OF THE DOPPLER SHIFT AND DELAY

In LEO mobile SatCom system, the satellites usually move along an approximately circular orbit of an altitude between 200km and 2000km. As the coverage of a LEO satellite is decided by the elevation angle, the satellite can communicate effectively with the UE only within a small percentage of the orbit period, namely the visibility window [13]. The Doppler shift f_d depends on the relative tangential velocity of the satellite with respect to the UE v, and the carrier frequency f_c, i.e.,

$$f_d = f_c \frac{v}{v_c} \tag{1}$$

where v_c is the speed of light. On the other hand, the fast relative movement between the satellite and the UE can cause variation of the propagation delay between the successive radio frames as well.

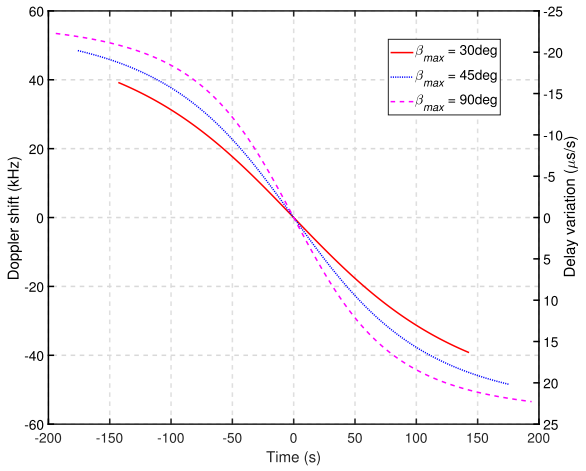

FIGURE 2. Doppler shift and communication delay variation characterization curves with the maximum elevation angle $\beta_{max} = 30°, 45°$ and $90°$.

Consider a LEO mobile SatCom system with a carrier frequency of 2.6GHz, a 600km altitude orbit, and the minimum elevation angle and the down-tilt angle being 10° and 60°, respectively, Fig.2 presents the Doppler shift value and the variation of propagation delay during the visible window. Three UE locations are observed with their maximum elevation angle being 30°, 45°, 90°, respectively. It can be observed that both the Doppler shift and the propagation delay variation are S-shaped curves as a function of time and the maximum elevation angle. The maximum absolute values of Doppler shift and propagation delay variation are about 55kHz and 20μs/s, respectively. For Ka-band LEO SatCom systems, there may exist a Doppler shift larger than 600kHz in the satellite-to-ground link.

Notice that the maximum values of the Doppler shift, the variation of the Doppler shift, and the variation of the propagation delay within the visibility window are determined by the parameters of the satellite orbit and UE locations. In this work, such characteristics will be utilized to develop the timing and frequency synchronization algorithm.

C. 5G NR SYNCHRONIZATION SIGNAL

CP-OFDM has been adopted as the basic waveform for 5G NR due to its high spectrum efficiency, and a frame structure compatible with the LTE system [32]. On the other hand,

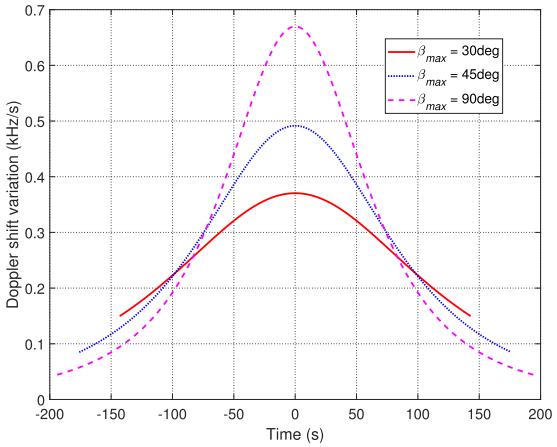

FIGURE 3. Doppler shift variation characterization curves with the maximum elevation angle $\beta_{max} = 30°, 45°$ and 90°.

TABLE 1. Parameters of the frame structure in NR.

μ	$f_{\text{scs}} = 2^{\mu} \cdot 15[\text{kHz}]$	CP type	$N_{\text{slot}}^{\text{subframe}}$	$N_{\text{symb}}^{\text{slot}}$
0	15	Normal	1	14
1	30	Normal	2	14
2	60	Normal	4	14
2	60	Extended	4	12
3	120	Normal	8	14
4	240	Normal	16	14

the length of the slot and OFDM symbol are variable and dependent on the chosen subcarrier spacing and CP type, which are shown in Table 1, where f_{scs} denotes the subcarrier spacing, $N_{\text{slot}}^{\text{subframe}}$ and $N_{\text{symb}}^{\text{slot}}$ denote the number of slots in one subframe and the number of OFDM symbols in one slot, respectively.

In the case that the subcarrier spacing is 30kHz, the corresponding frame structure is shown in Fig.4. In NR, the so-called synchronization signal block (SSB) is introduced, comprising the PSS, the secondary synchronization signals (SSS) and the physical broadcast channel (PBCH) signals. The UE can achieve time-frequency synchronization and acquire cell ID and other basic system information through the detection of the SSB. The PSS sequence occupying N_{pss} subcarriers in the frequency domain is generated by

$$d(k) = 1 - 2x\left(\left(k + 43N_{\text{ID}}^{(2)}\right)_{N_{\text{pss}}}\right) \tag{2}$$

where $k = 0, 1, \ldots N_{\text{pss}} - 1$, $N_{\text{pss}} = 127$ and $N_{\text{ID}}^{(2)}$ represents the physical-layer identity in the range of 0 to 2 in order to avoid collision of the same PSS from neighboring cells. The sequence $x(p)$ is recursively generated as follows

$$x(p+7) = (x(p+4) + x(p))_2 \tag{3}$$

where the initial value of $x(p)$ is given by

$$x(p) = \begin{cases} 0, & p = 0, 3, \\ 1, & p = 1, 2, 4, 5, 6. \end{cases} \tag{4}$$

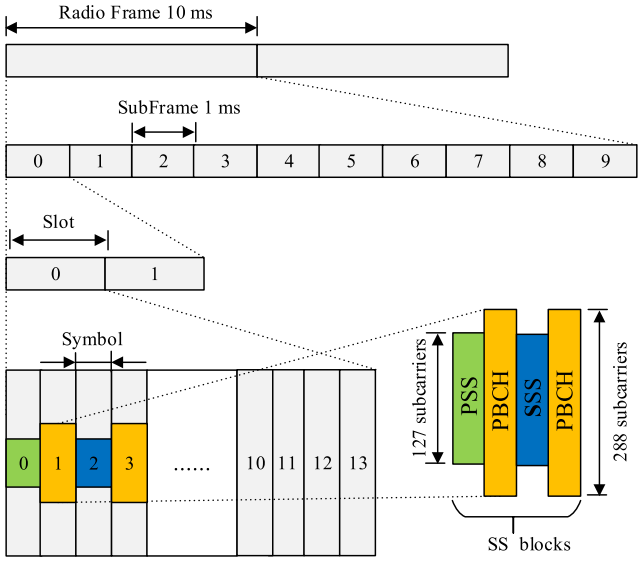

FIGURE 4. The frame structure of 5G NR for normal CP when the subcarrier spacing is 30 kHz.

Note that $x(p)$ is a m-sequence with a period of 127, which is favored for synchronization purposes due to its good correlation performance [33]. After mapping the length-N_{pss} m-sequence $d(k)$ onto the appropriate subcarriers in frequency domain, the desired discrete time-domain PSS $s_{\text{pss}}(n)$ can be defined as an OFDM symbol using an N-point inverse fast Fourier transformation (IFFT) as follows

$$s_{\text{pss}}(n) = \frac{1}{\sqrt{N_{\text{pss}}}} \sum_{k=k_0}^{k_0+N_{\text{pss}}-1} d(k-k_0) e^{\bar{\jmath}2\pi n(k-k_0)/N} \tag{5}$$

where $n = 0, 1, \ldots, N-1$ and k_0 denotes the starting point of OFDM symbol in the frequency domain. In addition, a CP should be added to $s_{\text{pss}}(n)$ before transmission.

D. TIMING AND FREQUENCY OFFSET

In the downlink of the 5G integrated LEO SatCom system, 5G NR CP-OFDM signals are assumed to be employed. Let N and N_g denote the number of subcarriers and length of CP, respectively. After inserting the CP at the beginning of each OFDM symbol to prevent ISI and preserve the mutual orthogonality of subcarriers, the m-th OFDM symbol $s_m(n)$ for $n = 0, 1, \ldots, N + N_g - 1$ is transmitted through the channel. Then, the received signal $r_m(n)$ can be given by

$$r_m(n) = e^{\bar{\jmath}2\pi n\varepsilon/N} \sum_{l=0}^{L-1} h(l) s_m(n - \theta - l) + z(n) \tag{6}$$

where ε is the normalized carrier frequency offset with respect to the subcarrier spacing, θ is the integer normalized symbol timing offset with respect to the sampling interval, $h(l)$ denotes the impulse response of a multipath channel with L uncorrelated taps, and $z(n)$ is the additive white Gaussian noise (AWGN) with zero mean and variance σ_z^2. To avoid ISI,

the channel length is assumed to be less than the CP length, i.e., $L < N_g$.

After removing the CP, the received sequence $r_m(n)$ can be stacked and represented in the vector form as

$$\mathbf{r}_m = \mathbf{D}(\varepsilon)\mathbf{S}_m\mathbf{h} + \mathbf{z} \tag{7}$$

where $\mathbf{r}_m$ is a $N \times 1$ vector with the i-th element being $r_m(\theta + N_g + i)$ for $i = 0, 1, \ldots, N-1$, $\mathbf{h} = [h(0), h(1), \ldots h(L-1)]^T$, the frequency offset matrix $\mathbf{D}(\varepsilon) \in \mathbb{C}^{N\times N}$ is diagonal with its n-th element being $e^{j2\pi\varepsilon(\theta+N_g+n-1)/N}$, $\mathbf{z}$ is the AWGN noise vector with zero mean and covariance matrix $\sigma_z^2\mathbf{I}_N$ and $\mathbf{S}_m$ is a $N \times L$ circulant matrix formed by transmitted signal $s_m(n)$ for $n = N_g, N_g + 1, \ldots, N + N_g - 1$.

The timing and frequency synchronization aim to get the estimates of the unknown parameters θ and ε by exploiting the observation $r_m(n)$ at the receiver. However, on account of the large Doppler frequency shift in satellite-ground links and the unknown channel coefficient $\mathbf{h}$, the estimation becomes a challenging task. Based on the Doppler shift characteristics and synchronization signal model given in this section, our research focuses on time-frequency synchronization problems under large frequency offset in the following.

III. INITIAL SYNCHRONIZATION

The initial synchronization is to estimate the timing and frequency offset without any prior information. To this end, both the PSS and the CP of OFDM can be utilized. In this section, we first develop a new timing and frequency offset estimation algorithm only with the PSS, then investigate how to utilize the CP to improve the performance further.

A. INITIAL SYNCHRONIZATION ONLY WITH PSS

Without loss of generality, we assume that the PSS is transmitted on the first OFDM symbol, which leads to

$$\mathbf{r}_0 = \mathbf{X}\mathbf{h} + \mathbf{z} \tag{8}$$

where $\mathbf{X}$ is defined as $\mathbf{X} = \mathbf{D}(\varepsilon)\mathbf{S}_0$ for notational clarity. Note that $\mathbf{S}_0^H\mathbf{S}_0 = N\mathbf{I}_L$ since the PSS is generated by the m-sequence with the property of cyclic autocorrelation.

Since the joint estimation of θ, ε and $\mathbf{h}$ is computationally infeasible, we first consider the maximum log-likelihood timing offset estimation alternatively, i.e.,

$$\hat{\theta} = \arg\max_{\theta} \log f(\mathbf{r}_0|\theta) \tag{9}$$

where $f(\mathbf{r}_0|\theta)$ is the conditional probability density function of $\mathbf{r}_0$ given θ. In addition, the conditional probability density function of $\mathbf{r}_0$ given θ, ε and $\mathbf{h}$ is given by

$$f(\mathbf{r}_0|\theta, \varepsilon, \mathbf{h}) = \frac{1}{\left(\pi\sigma_z^2\right)^N} \exp\left\{-\frac{|\mathbf{r}_0 - \mathbf{X}\mathbf{h}|^2}{\sigma_z^2}\right\}. \tag{10}$$

Then, the likelihood function can be calculated by

$$f(\mathbf{r}_0|\theta) = \int f(\mathbf{r}_0|\theta, \varepsilon, \mathbf{h}) f(\varepsilon, \mathbf{h}|\theta)\, d\varepsilon d\mathbf{h} \tag{11}$$

where $f(\varepsilon, \mathbf{h}|\theta)$ is the joint probability density function of ε and $\mathbf{h}$ given θ. However, since the above integral is difficult to compute, the ML estimation of timing offset can not be solved effectively. In the following, we will develop an upper bound of $\log f(\mathbf{r}_0|\theta)$ and then maximize it with respect to θ to obtain the estimation of the timing offset.

According to the Bayesian formula, we have

$$\begin{aligned} f(\mathbf{r}_0, \theta, \varepsilon, \mathbf{h}) &= f(\theta) f(\mathbf{r}_0|\theta) f(\varepsilon, \mathbf{h}|\mathbf{r}_0, \theta) \\ &= f(\theta) f(\varepsilon, \mathbf{h}|\theta) f(\mathbf{r}_0|\theta, \varepsilon, \mathbf{h}) \end{aligned} \tag{12}$$

where $f(\theta)$ is the probability density function of θ and $f(\varepsilon, \mathbf{h}|\mathbf{r}_0, \theta)$ is the conditional probability density function of ε, $\mathbf{h}$ given $\mathbf{r}_0$, θ. We then obtain

$$f(\mathbf{r}_0|\theta) = \frac{f(\mathbf{r}_0|\theta, \varepsilon, \mathbf{h}) f(\varepsilon, \mathbf{h}|\theta)}{f(\varepsilon, \mathbf{h}|\mathbf{r}_0, \theta)}. \tag{13}$$

Applying the log operation to both sides of (13), we obtain

$$\log f(\mathbf{r}_0|\theta) = \log f(\mathbf{r}_0|\theta, \varepsilon, \mathbf{h}) - \log \frac{f(\varepsilon, \mathbf{h}|\mathbf{r}_0, \theta)}{f(\varepsilon, \mathbf{h}|\theta)}. \tag{14}$$

Then, we can easily derive an upper bound of $\log f(\mathbf{r}_0|\theta)$ provided in the following theorem.

Theorem 1: An upper bound of $\log f(\mathbf{r}_0|\theta)$ can be obtained by

$$\log f(\mathbf{r}_0|\theta) \le \int \log f(\mathbf{r}_0|\theta, \varepsilon, \mathbf{h}) f(\varepsilon, \mathbf{h}|\mathbf{r}_0, \theta)\, d\varepsilon d\mathbf{h} \tag{15}$$

Proof: The proof is given in Appendix. ■

However, the explicit expression of $f(\varepsilon, \mathbf{h}|\mathbf{r}_0, \theta)$ is still difficult to obtain. Thus, here we try to obtain reasonable simplification alternatively. According to the Bayesian formula, we have

$$f(\varepsilon, \mathbf{h}|\mathbf{r}_0, \theta) = f(\varepsilon|\mathbf{r}_0, \theta) f(\mathbf{h}|\mathbf{r}_0, \theta, \varepsilon). \tag{16}$$

Considering the characteristic of the Doppler frequency shift mentioned in section II that the Doppler shift is limited in the finite amplitude by visibility window, i.e., $\varepsilon_1 \le \varepsilon \le \varepsilon_2$, we assume that ε is uniformly distributed within $[\varepsilon_1, \varepsilon_2]$ and the corresponding probability density function is given by

$$f(\varepsilon|\mathbf{r}_0, \theta) = \begin{cases} \dfrac{1}{\varepsilon_2 - \varepsilon_1}, & \varepsilon \in [\varepsilon_1, \varepsilon_2], \\ 0, & \text{otherwise}, \end{cases} \tag{17}$$

On the other hand, it is difficult to obtain actual distribution $f(\mathbf{h}|\mathbf{r}_0, \theta, \varepsilon)$ in (16) before initial synchronization as well. Here we use the maximum log-likelihood estimation value of $\mathbf{h}$ instead, i.e., $f(\mathbf{h}|\mathbf{r}_0, \theta, \varepsilon) = \delta\left(\mathbf{h} - \hat{\mathbf{h}}\right)$, where $\hat{\mathbf{h}}$ can be easily obtained from (7) by

$$\begin{aligned} \hat{\mathbf{h}} &= \arg\max_{\mathbf{h}} \log f(\mathbf{r}_0|\theta, \varepsilon, \mathbf{h}) \\ &= \left(\mathbf{X}^H\mathbf{X}\right)^{-1}\mathbf{X}^H\mathbf{r}_0 \end{aligned} \tag{18}$$

Hence, the conditional probability density function $f(\varepsilon, \mathbf{h}|\mathbf{r}_0, \theta)$ in (16) becomes

$$f(\varepsilon, \mathbf{h}|\mathbf{r}_0, \theta) = \frac{1}{\varepsilon_2 - \varepsilon_1}\delta\left(\mathbf{h} - \hat{\mathbf{h}}\right). \tag{19}$$

With (19), the upper bound in (15) can be approximated by

$$U = \frac{1}{\varepsilon_1 - \varepsilon_2} \int_{\varepsilon_1}^{\varepsilon_2} \log f\left(\mathbf{r}_0 | \theta, \varepsilon, \hat{\mathbf{h}}\right) d\varepsilon. \tag{20}$$

Thus, the optimization problem of timing offset becomes

$$\begin{aligned} \hat{\theta} &= \arg\max_{\theta} \int_{\varepsilon_1}^{\varepsilon_2} \log f\left(\mathbf{r}_0 | \theta, \varepsilon, \hat{\mathbf{h}}\right) d\varepsilon \\ &\overset{(a)}{=} \arg\max_{\theta} \int_{\varepsilon_1}^{\varepsilon_2} \mathbf{r}_0^H \mathbf{X}\left(\mathbf{X}^H \mathbf{X}\right)^{-1} \mathbf{X}^H \mathbf{r}_0 d\varepsilon \\ &\overset{(b)}{=} \arg\max_{\theta} \int_{\varepsilon_1}^{\varepsilon_2} \left|\mathbf{S}_0^H \mathbf{D}^H(\varepsilon) \mathbf{r}_0\right|^2 d\varepsilon \\ &\triangleq \arg\max_{\theta} \ \psi(\theta) \end{aligned} \tag{21}$$

where $\overset{(a)}{=}$ holds based on (10) and (18), and $\overset{(b)}{=}$ holds due to $\mathbf{X} = \mathbf{D}(\varepsilon)\mathbf{S}_0$ and $\mathbf{S}_0^H \mathbf{S}_0 = N\mathbf{I}_L$. Furthermore, $\psi(\theta)$ can be expressed equivalently as

$$\begin{aligned} \psi(\theta) &= \sum_{l_1, l_2 = 0}^{L-1} \sum_{i,j=0}^{N-1} \eta(i, l_1)\, \eta^*(j, l_2) \int_{\varepsilon_1}^{\varepsilon_2} e^{\bar{\jmath} 2\pi \varepsilon (i-j)/N} d\varepsilon \\ &= \boldsymbol{\alpha}^H \mathbf{A} \boldsymbol{\alpha} \end{aligned} \tag{22}$$

where

$$\eta(i, l) = s_0\left(N_g + (i - l)_N\right) r_0^*\left(\theta + N_g + i\right) \tag{23}$$

for $l = 0, 1, \ldots, L-1$ and

$$\boldsymbol{\alpha} = \mathbf{r}_0 \odot \sum\nolimits_{l=0}^{L-1} \mathbf{s}_l^* \tag{24}$$

where $\mathbf{s}_l$ denotes the l-th column vector of $\mathbf{S}_0$. The entries of $\mathbf{A} \in \mathbb{C}^{N \times N}$ in (22) can be given by

$$\begin{aligned} [\mathbf{A}]_{ij} &= \int_{\varepsilon_1}^{\varepsilon_2} e^{\bar{\jmath} 2\pi \varepsilon (i-j)/N} d\varepsilon \\ &= N 2w \operatorname{sinc}\left(2w(i-j)\right) e^{\bar{\jmath} 2\pi \varphi (i-j)} \end{aligned} \tag{25}$$

where $i, j = 0, 1, \ldots, N-1$ and

$$w = \frac{\varepsilon_2 - \varepsilon_1}{2N}, \tag{26}$$

$$\varphi = \frac{\varepsilon_2 + \varepsilon_1}{2N}. \tag{27}$$

The eigenvectors of the matrix $\mathbf{A}$ are the modulated DPSS basis [34]. Before presenting the decomposition, we review the definition and several important properties of the modulated DPSS basis as follows.

DPSS [35]: Given an integer a and a parameter $\kappa \in (0, 0.5)$, the DPSS vectors $\mathbf{u}_{a,\kappa}^{(0)}, \mathbf{u}_{a,\kappa}^{(1)}, \ldots, \mathbf{u}_{a,\kappa}^{(a-1)} \in \mathbb{R}^a$ and the corresponding DPSS eigenvalues $\lambda_{a,\kappa}^{(0)}, \lambda_{a,\kappa}^{(1)}, \ldots, \lambda_{a,\kappa}^{(a-1)}$, with order $1 > \lambda_{a,\kappa}^{(0)} > \lambda_{a,\kappa}^{(1)} > \ldots > \lambda_{a,\kappa}^{(a-1)} > 0$, satisfy

$$\mathbf{B}_{a,\kappa} \mathbf{u}_{a,\kappa}^{(p)} = \lambda_{a,\kappa}^{(p)} \mathbf{u}_{a,\kappa}^{(p)} \tag{28}$$

where $\mathbf{B}_{a,\kappa} \in \mathbb{C}^{a \times a}$ is the prolate matrix with elements

$$\left[\mathbf{B}_{a,\kappa}\right]_{pq} = 2\kappa \operatorname{sinc}\left(2\kappa(p-q)\right) \tag{29}$$

for $p, q = 0, 1, \ldots, a-1$. Let $\mathbf{U}_{a,\kappa} \in \mathbb{C}^{a \times a}$ denote the matrix whose p-th column is the DPSS vector $\mathbf{u}_{a,\kappa}^{(p)}$ and $\boldsymbol{\Lambda}_{a,\kappa} \in \mathbb{C}^{a \times a}$ denote a diagonal matrix with the DPSS eigenvalues sorted in descending order along the main diagonal. The prolate matrix $\mathbf{B}_{a,\kappa}$ can be factorized as

$$\mathbf{B}_{a,\kappa} = \mathbf{U}_{a,\kappa} \boldsymbol{\Lambda}_{a,\kappa} \mathbf{U}_{a,\kappa}^H \tag{30}$$

which is an eigendecomposition of the matrix $\mathbf{B}_{a,\kappa}$. The eigenvalues $\lambda_{a,\kappa}^{(0)}, \lambda_{a,\kappa}^{(1)}, \ldots, \lambda_{a,\kappa}^{(a-1)}$ have a very distinctive and important characteristic: the first $2a\kappa$ eigenvalues tend to cluster close to 1, while most of the remaining eigenvalues tend to cluster close to 0, only a small number of eigenvalues lying in between [34], [35]. This characteristic will allow us to construct efficient bases using small numbers of DPSS vectors. Furthermore, the definition of modulated DPSS dictionary can be given as follows [34].

Modulated DPSS: Given the DPSS matrix $\mathbf{U}_{a,\kappa} \in \mathbb{C}^{a \times a}$, the modulated DPSS matrix $\mathbf{V}_{\kappa,\vartheta} \in \mathbb{C}^{a \times a}$ can be obtained by

$$\mathbf{V}_{\kappa,\vartheta} = \mathbf{E}_{a,\vartheta} \mathbf{U}_{a,\kappa} \tag{31}$$

where ϑ is the modulating parameter and $\mathbf{E}_{a,\vartheta}$ denotes a $a \times a$ diagonal matrix with entries

$$[\mathbf{E}_{a,\vartheta}]_{pq} = \begin{cases} e^{\bar{\jmath} 2\pi p \vartheta}, & p = q \\ 0, & p \neq q \end{cases} \tag{32}$$

for $p, q = 0, 1, \ldots, a-1$.

With the definitions of the modulated DPSS matrix, the matrix $\mathbf{A}$ in (25) can be dealt with in the following way. Since N is always much greater than $(\varepsilon_2 - \varepsilon_1)$, the parameter w in (26) satisfies $w \in (0, 0.5)$. From (25) (30) and (31), the matrix $\mathbf{A}$ can be reexpressed as

$$\begin{aligned} \mathbf{A} &= N \mathbf{E}_{N,\varphi} \mathbf{B}_{N,w} \mathbf{E}_{N,\varphi}^H \\ &= N \mathbf{E}_{N,\varphi} \mathbf{U}_{N,w} \boldsymbol{\Lambda}_{N,w} \mathbf{U}_{N,w}^H \mathbf{E}_{N,\varphi}^H \\ &= N \mathbf{V}_{w,\varphi} \boldsymbol{\Lambda}_{N,w} \mathbf{V}_{w,\varphi}^H. \end{aligned} \tag{33}$$

By substituting (33) into (22), $\psi(\theta)$ becomes

$$\begin{aligned} \psi(\theta) &= \boldsymbol{\alpha}^H \left(N \mathbf{V}_{w,\varphi} \boldsymbol{\Lambda}_{N,w} \mathbf{V}_{w,\varphi}^H\right) \boldsymbol{\alpha} \\ &= N \sum_{i=0}^{N-1} \lambda_{N,w}^{(i)} \left|\mathbf{v}_i^H \boldsymbol{\alpha}\right|^2 \\ &\overset{(a)}{=} N \sum_{i=0}^{N-1} \lambda_{N,w}^{(i)} \left| \left(\mathbf{v}_i \odot \sum_{l=0}^{L-1} \mathbf{s}_l\right)^H \mathbf{r}_0 \right|^2 \\ &\overset{(b)}{\approx} N \sum_{i=0}^{K-1} \left| \left(\mathbf{v}_i \odot \sum_{l=0}^{L-1} \mathbf{s}_l\right)^H \mathbf{r}_0 \right|^2 \end{aligned} \tag{34}$$

where $\mathbf{v}_i \in \mathbb{C}^{N \times 1}$ denotes the i-th column vector of $\mathbf{V}_{w,\varphi}$ and K is the integer portion of $2Nw$. $\overset{(a)}{=}$ is based on (24) and $\overset{(b)}{\approx}$ is a tight lower bound due to the property of these eigenvalues reviewed in definition of DPSS. Hence by omitting the parameter N the estimate of θ based on PSS can be finally

obtained by

$$\hat{\theta} = \Lambda_{pss}(\theta) = \arg\max_{\theta} \sum_{i=0}^{K-1} \lambda_{N,w}^{(i)} \left| \left(\mathbf{v}_i \odot \sum_{l=0}^{L-1} \mathbf{s}_l \right)^H \mathbf{r}_0 \right|^2 \quad (35a)$$

$$\approx \arg\max_{\theta} \sum_{i=0}^{K-1} \left| \left(\mathbf{v}_i \odot \sum_{l=0}^{L-1} \mathbf{s}_l \right)^H \mathbf{r}_0 \right|^2 \quad (35b)$$

This approximation reduces the computational complexity greatly, meanwhile the numerical simulations indicate that this approximate scheme can also work effectively.

It shall be noted that when there is no frequency offset in system, $\mathbf{v}_i$ is transformed into a vector of all ones, hence the proposed timing estimation scheme is degenerated into the conventional cross-correlation based estimation algorithm [25]–[29]. Consequently, the proposed method is structurally compatible compared to the conventional cross-correlation method.

When the time synchronization has been achieved, we consider the frequency offset estimation. In the same way, the optimization problem based on the maximum log-likelihood criterion can be expressed as

$$\hat{\varepsilon} = \arg\max_{\varepsilon} \log f(\mathbf{r}_0|\varepsilon) \quad (36)$$

where $f(\mathbf{r}_0|\varepsilon)$ is the conditional probability density function of $\mathbf{r}_0$ given ε. Similar to the estimation of timing offset and using the ML estimation value $\hat{\mathbf{h}} = \left(\mathbf{X}^H\mathbf{X}\right)^{-1}\mathbf{X}^H\mathbf{r}_0$, (36) becomes

$$\hat{\varepsilon} = \arg\max_{\varepsilon} \log f\left(\mathbf{r}_0|\hat{\theta}, \varepsilon, \hat{\mathbf{h}}\right). \quad (37)$$

Omitting the factors independent of ε, the optimization problem shown in (37) becomes

$$\hat{\varepsilon} = \arg\max_{\varepsilon} \Upsilon_{pss}\left(\hat{\theta}, \varepsilon\right) \quad (38)$$

where $\Upsilon_{pss}\left(\hat{\theta}, \varepsilon\right)$, the objective function of frequency offset, can be given by

$$\Upsilon_{pss}\left(\hat{\theta}, \varepsilon\right) = \left|(\mathbf{D}(\varepsilon)\mathbf{S}_0)^H\mathbf{r}_0\right|^2 = \left| \left(\mathbf{d}(\varepsilon) \odot \sum_{l=0}^{L-1} \mathbf{s}_l \right)^H \mathbf{r}_0 \right|^2 \quad (39)$$

with $[\mathbf{d}(\varepsilon)]_i = e^{-\bar{\jmath}2\pi\varepsilon i/N}$ for $i = 0, 1, \ldots, N-1$.

In (38), a grid search is used to estimate the large frequency offset. However the resulting complexity makes the implementation of this frequency offset estimation method infeasible. We further observe that the redundancy of CP in OFDM symbol can be exploited in timing and frequency offset estimation similarly. Hence, based on the proposed PSS algorithm, we consider utilizing the CP as auxiliary information to improve the estimation performance and avoid the involved one-dimensional exhaustive search in the frequency offset estimation.

B. CP ASSISTED PSS ALGORITHM

Assuming that we observe $(N + N_g - L + 1)$ consecutive samples of $r_m(n)$, the received sequence can be stacked and represented in vector form as $\mathbf{r}'_m$, whose i-th element is $r_m(\theta + L - 1 + i)$ for $i = 0, 1, \ldots, N + N_g - L$. Since the joint maximum log-likelihood estimation of θ and ε is the argument maximizing its log-likelihood function, considering the CP in multiple OFDM symbols, we can get the following estimation expression

$$\left(\hat{\theta}, \hat{\varepsilon}\right) = \arg\max_{\theta,\varepsilon} \log \prod_m f\left(\mathbf{r}'_m|\theta, \varepsilon\right) \quad (40)$$

where $f\left(\mathbf{r}'_m|\theta, \varepsilon\right)$ is the probability density function of the observed samples $\mathbf{r}'_m$ given the arrival time θ and the carrier frequency offset ε. Discarding the terms independent of θ and ε, log-likelihood function of θ and ε can be expressed as [20], [24]

$$\log \prod_m f\left(\mathbf{r}'_m|\theta, \varepsilon\right) = \sum_m \left(2\Gamma_m(\theta, \varepsilon) - \rho\Phi_m(\theta)\right) \quad (41)$$

where

$$\Gamma_m(\theta, \varepsilon) = \sum_{n\in I} \mathrm{Re}\left\{e^{\bar{\jmath}2\pi\varepsilon} r_m(n) r_m^*(n+N)\right\}, \quad (42)$$

$$\Phi_m(\theta) = \sum_{n\in I} \left(|r_m(n)|^2 + |r_m(n+N)|^2\right). \quad (43)$$

where $I = \left\{\theta + L - 1, \ldots, \theta + N_g - 1\right\}$ is the index set of CP part. The parameter ρ in (41) representing the amplitude of the correlation coefficient is given by

$$\rho = \left| \frac{\mathbb{E}\left\{r_m(n) r_m^*(n+N)\right\}}{\sqrt{\mathbb{E}\left\{|r_m(n)|^2\right\}\mathbb{E}\left\{|r_m(n+N)|^2\right\}}} \right| = \frac{\sigma^2}{\sigma^2 + \sigma_z^2} = \frac{\mathrm{SNR}}{\mathrm{SNR} + 1} \quad (44)$$

where $\sigma^2 = \sigma_s^2 \sum_{l=0}^{L-1} |h(l)|^2$ and $\sigma_s^2 = \mathbb{E}\left\{|s_m(n)|^2\right\}$ represent the received signal power and transmitted signal power respectively, $\mathrm{SNR} = \sigma^2/\sigma_z^2$ denotes the signal-to-noise ratio (SNR) in receiver. Notice that $\Gamma_m(\theta, \varepsilon)$ can be rewritten as

$$\Gamma_m(\theta, \varepsilon) = |\xi_m(\theta)| \cos\left(2\pi\varepsilon + \angle\xi_m(\theta)\right) \quad (45)$$

$$\xi_m(\theta) = \sum_{n\in I} r_m(n) r_m^*(n+N) \quad (46)$$

The term $\Phi_m(\theta)$ in (41) is an energy term, independent of the frequency offset. Therefore, estimation argument maximizing $\log \prod_m f\left(\mathbf{r}'_m|\theta, \varepsilon\right)$ can be obtained by letting the cosine function term in (45) be equal to unity [20], [24]

$$\cos\left(2\pi\varepsilon + \angle\xi_m(\theta)\right) = 1. \quad (47)$$

Hence $\Lambda_{cp}(\theta)$, the compressed log-likelihood function with respect to ε, can be given by

$$\Lambda_{cp}(\theta) = \sum_m \left(2|\xi_m(\theta)| - \rho\Phi_m(\theta)\right). \quad (48)$$

On the basis of timing offset estimation in previous PSS algorithm, we further take advantage of CP to improve the estimation accuracy of timing offset as follows

$$\hat{\theta} = \arg\max_{\theta} \ \Lambda_{pss}(\theta) \ \text{ s.t. } \ \Lambda_{cp}(\theta) \geq \Im \tag{49}$$

where the parameter $\Im$ is the threshold decided by the channel quality and performance requirements. The scheme in (49) actually conducts the coarse timing offset estimation with CP and fine timing offset estimation with PSS, respectively.

When the timing offset θ is estimated, the estimate of frequency offset ε can be obtained by utilizing both multiple CPs and PSS as follows. Considering the periodicity of cosine function based on (47), the estimate of the fractional frequency offset ε_{ffo} can be obtained by [20]

$$\hat{\varepsilon}_{ffo} = -\frac{1}{2\pi} \angle \sum_{m} \xi_m(\hat{\theta}). \tag{50}$$

Since we have got the fractional frequency offset, the whole carrier frequency offset can be obtained by

$$\begin{aligned} \hat{\varepsilon} &= \arg\max_{\varepsilon} \ \Upsilon_{pss}\left(\hat{\theta}, \varepsilon\right) \\ &\text{s.t. } \ \hat{\varepsilon}_{ffo} = -\frac{1}{2\pi} \angle \sum_{m} \xi_m(\hat{\theta}). \end{aligned} \tag{51}$$

When the FFO is estimated, we only need to search CFO among a few carrier frequency offsets using the proposed PSS algorithm over the frequency offset range. Compared to the proposed estimation method of frequency offset in (38), the CP assisted algorithm in (51) significantly reduces the complexity of the estimation, thus making the frequency offset estimation method feasible in practical application.

It is worth noting that, according to the simulation results, CP assisted algorithm has limited performance improvement for timing offset estimation compared with that of PSS algorithm, and the performance of latter can already meet the requirements of the communication system. In terms of frequency offset estimation, with the aid of CP, the complexity of frequency offset estimation can be reduced while the synchronization performance can be improved. Therefore, we can use the following combination to estimate the timing and frequency offset

$$\hat{\theta} = \arg\max_{\theta} \ \Lambda_{pss}(\theta), \tag{52}$$

$$\begin{aligned} \hat{\varepsilon} &= \arg\max_{\varepsilon} \ \Upsilon_{pss}\left(\hat{\theta}, \varepsilon\right) \\ &\text{s.t. } \ \hat{\varepsilon}_{ffo} = -\frac{1}{2\pi} \angle \sum_{m} \xi_m(\hat{\theta}). \end{aligned} \tag{53}$$

The synchronization algorithm presented in (52) and (53) can be denoted by DPSS assisted algorithm for notational clarity.

Considering the channel length L used in the proposed methods presented above, we can assume $L = 1$ in initial synchronization. After achieving the coarse synchronization and getting the value of L according to statistical channel information, we then apply it to the proposed methods again to achieve the fine synchronization.

IV. TRACKING SYNCHRONIZATION

After the communication system has synchronized in the initial synchronization, it is still difficult to maintain the achieved synchronization state because the satellite is moving at a very high speed and the channel environment in satellite-ground links is time-varying. Thus, based on the achieved initial synchronization, the LEO mobile SatCom system enters the tracking synchronization where UE continuously tracks the change of the parameters including timing and frequency offset and makes the corresponding adjustments. Compared to the initial synchronization, the tracking synchronization is conducted in each SSB, which puts forward higher requirements for the complexity of the timing and frequency offset estimation algorithm.

As mentioned in section II, for LEO mobile SatCom system with a certain orbit altitude, the maximum variation rate of Doppler frequency shift and communication delay can be approximately obtained, and the time delay and frequency offset of received signal change little between adjacent SSBs. During each tracking synchronization process, we first compensate the frequency offset for the received signal with the estimated frequency offset in the last tracking synchronization. After the frequency offset compensation, the residual carrier frequency offset is restricted to a small fraction which is nearly zero since the change of Doppler shift is quite small between successive SSBs. Therefore, the timing offset in the $(k+1)$-th tracking synchronization can be estimated as follows

$$\begin{aligned} \hat{\theta}_{k+1} &= \arg\max_{\theta_{k+1}} \ \log f\left(\mathbf{r}_0 | \theta_{k+1}, \hat{\mathbf{h}}, \varepsilon_{k+1} = 0\right) \\ &= \arg\max_{\theta_{k+1}} \left| \mathbf{r}_0^H \sum\nolimits_{l=0}^{L-1} \mathbf{s}_l \right|^2. \end{aligned} \tag{54}$$

Let $\Delta\tau$ denotes the maximum communication delay variation between two adjacent SSBs, the corresponding normalized timing offset variation can be obtained as

$$\Delta\theta = \Delta\tau / T_s \tag{55}$$

where T_s is the sampling interval. Hence, the timing offset of $(k+1)$-th tracking synchronization locates within the following range

$$\theta_{k+1} \in \left(\hat{\theta}_k - \Delta\theta, \hat{\theta}_k + \Delta\theta\right). \tag{56}$$

where $\hat{\theta}_0$ represents the initial synchronization timing offset estimation. Obviously, except for the initial synchronization requires a global blind timing search, subsequent tracking synchronization only needs to perform a small-scale search within the range shown in (56). With the help of the maximum communication delay variation, the tracking of the timing offset can be conducted with low-complexity.

When the timing offset is estimated, the residual carrier frequency offset can be further estimated as follows

$$\hat{\varepsilon}_{k+1} = -\frac{1}{2\pi} \angle \sum_{m} \xi_m(\hat{\theta}_{k+1}). \tag{57}$$

Compared to initial synchronization, the estimation of frequency offset in tracking synchronization can exploit less number of CPs since the time synchronization is more accurate.

V. SIMULATION RESULTS

In this section, simulation results are provided to show the performance of the proposed estimation algorithms in initial and tracking synchronization. For initial synchronization, DPSS assisted algorithm, DPSS-S algorithm and CP-DPSS algorithm are all considered, where the DPSS assisted algorithm and the DPSS-S algorithm are based on (35a) and the approximation in (35b), respectively, and the CP-DPSS algorithm uses (49) to estimate the timing offset and (51) to estimate the frequency offset, respectively. For ease of comparison, the following two synchronization algorithms are also considered in the simulations.

- *Cross-correlation bound algorithm:* The method using (21) to estimate the timing offset with no frequency offset and using (38) to estimate the frequency offset with no timing offset.
- *CP-PSS-Optimal algorithm:* The method using (51) to estimate the frequency offset with no timing offset.

Note that the above two optimal methods both conduct one-dimensional grid searching of timing and frequency offset to get the corresponding parameter estimates.

In addition, the SNR at the receiver varies with the distance between the satellite and UE in the visibility window and directly affects the performance of proposed estimation algorithms. For the simulation of tracking synchronization, the dynamic SNR in downlink can be calculated as

$$\mathrm{SNR} = (\mathrm{EIRP})_{tx} + (G/T)_{rx} - L_{free} - L_{other} - k_{Bol} - 10\lg B \quad (58)$$

where $(\mathrm{EIRP})_{tx}$ denotes the effective isotropic radiated power of the satellite antenna, L_{free} denotes the free space loss, L_{other} denotes the propagation loss caused by rain attenuation, B denotes the system bandwidth, and k_{Bol} denotes the Boltzmann constant. $(G/T)_{rx}$ denotes the figure of merit of the receiver where G is the receiver antenna gain, and T is the equivalent system temperature. Note that the unit of SNR in (58) is decibel (dB).

The performance of synchronization algorithms is investigated by simulation with parameters summarized in Table 2. Note that even though multiple SSBs are contained in half radio frame according to 5G NR [32], we still employ one SSB within half radio frame in the simulation for a fair comparison. For CP assisted synchronization, the CP portion of 10 OFDM symbols are utilized, where one slot consists of 14 OFDM symbols. We follow the satellite-to-ground channel model defined in [9] which is a tapped delay line (TDL) model, where a multipath fading channel with 3.5GHz carrier frequency is adopted, and the channel parameters are summarized in Table 3. Note that the presented TDL model is applied in a suburban non-line of sight (NLOS) environment for UE with the maximum elevation angle $\beta_{max} = 30°$. For a system operating in high frequencies, the AWGN channel with 20GHz carrier frequency is adopted. In addition, for fairness, the normalized CFO present in both AWGN and multipath fading channels are randomly generated from the range $\varepsilon \in [3, 4]$.

TABLE 2. Parameters used in the simulation.

Parameter	Value	
Channel model	AWGN	Multipath
Carrier frequency	20GHz	3.5GHz
Subcarrier spacing	120kHz	15kHz
CFO	405.6kHz	50.7kHz
System bandwidth	480MHz	20MHz
Number of subcarriers	4096	2048
Sampling frequency	491.52MHz	30.72MHz
Synchronization signal	PSS in 5G NR	
CP type	Normal	
Number of antennas	1 Tx and 1 Rx	
Number of simulated frames	4000	

TABLE 3. Parameters in tapped delay line model [9].

Tap number	Normalized delay	Power (dB)	Fading distribution
1	0	-0.77	Rayleigh
2	0.53	0	Rayleigh
3	1.05	-5.71	Rayleigh
4	2.45	-3.83	Rayleigh
5	3.47	-8.97	Rayleigh

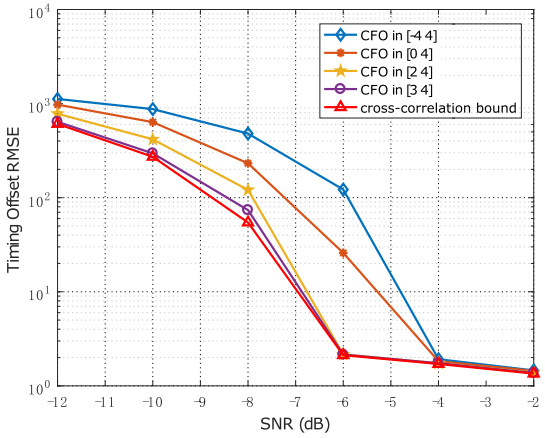

FIGURE 5. The timing offset estimation performance of the DPSS assisted algorithm with different frequency offset range over the AWGN channel.

The performance of the proposed methods is affected by the selected frequency offset range. Fig.5 and Fig.6 show the timing offset estimation performance of the DPSS assisted algorithm with different normalized frequency offset ranges in different environments, respectively. It can be observed that for the case with a large frequency offset range up to ± 4 normalized subcarrier spacings in initial

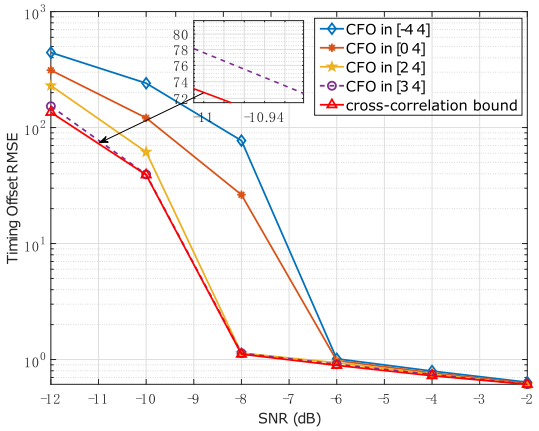

FIGURE 6. The timing offset estimation performance of the DPSS assisted algorithm with different frequency offset range over the multipath fading channel.

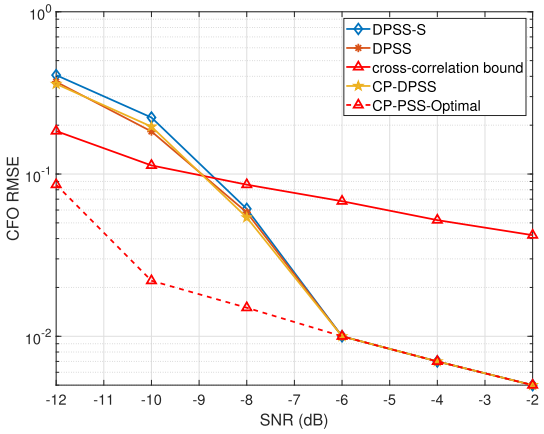

FIGURE 8. Frequency offset estimation performance comparison of different schemes over AWGN channel with $\varepsilon \in [2, 4]$.

synchronization, the time synchronization can be realized accurately (close to the optimal performance) after SNR $= -4$dB and SNR $= -6$dB for the AWGN and multipath fading channel, respectively. Furthermore, when the set frequency offset search range is one normalized subcarrier spacing, the timing performance of the DPSS assisted algorithm is close to the optimal performance.

For a specific frequency offset range, i.e., $\varepsilon \in [2, 4]$, the performance comparison of different schemes for the 5G NR downlink are shown in Figs.7-10.

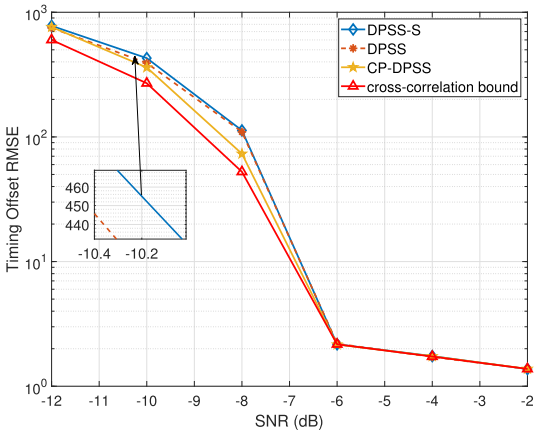

FIGURE 7. Timing offset estimation performance comparison of different schemes over AWGN channel with $\varepsilon \in [2, 4]$.

As can be seen, the performance of DPSS-S algorithm is rather close to the DPSS assisted algorithm, and the former has a simplified timing offset estimation. For the algorithms exploiting CP in frequency offset estimation, the frequency offset estimation performance can be close to its optimal performance and improved significantly compared to the performance of cross-correlation bound algorithm with the increase of SNR, which depicts that utilizing both the redundancy of CP in multiple OFDM symbols and PSS can achieve considerable advances in frequency synchronization. In addition,

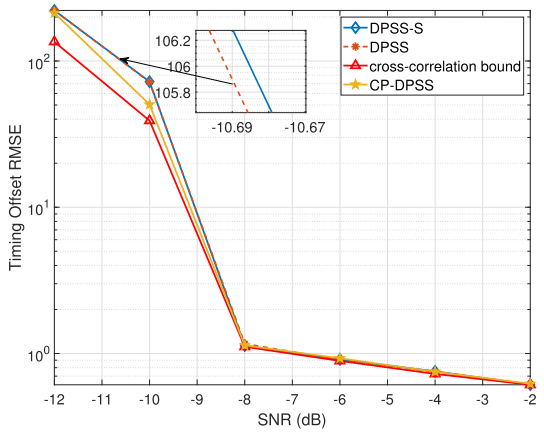

FIGURE 9. Timing offset estimation performance comparison of different schemes over multipath fading channel with $\varepsilon \in [2, 4]$.

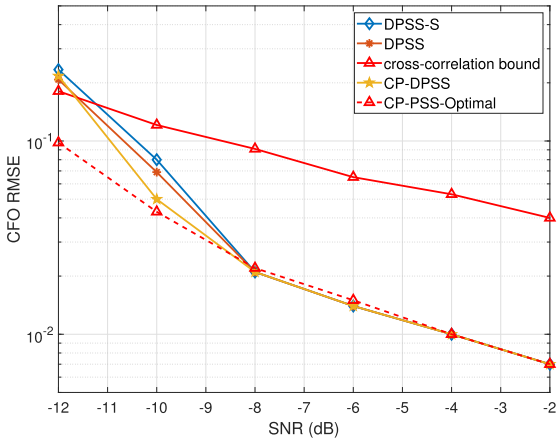

FIGURE 10. Frequency offset estimation performance comparison of different schemes over multipath fading channel with $\varepsilon \in [2, 4]$.

compared the timing offset estimation performance of CP-DPSS algorithm and DPSS assisted algorithm, the former does not improve the performance significantly. Specifically, the timing offset estimation error of the DPSS assisted algorithm can be up to 1.1 sampling intervals for AWGN channel

(when SNR $= -6$dB) and multipath fading channel (when SNR $= -8$dB), and the frequency offset estimation error can be up to 6% of the subcarrier spacing for AWGN channel (when SNR $= -8$dB) and 2% of the subcarrier spacing for multipath fading channel (when SNR $= -8$dB), which can meet the synchronization error requirements of OFDM system [10], [20]. Hence, the DPSS assisted algorithm or the DPSS-S algorithm can be good choices in practical application.

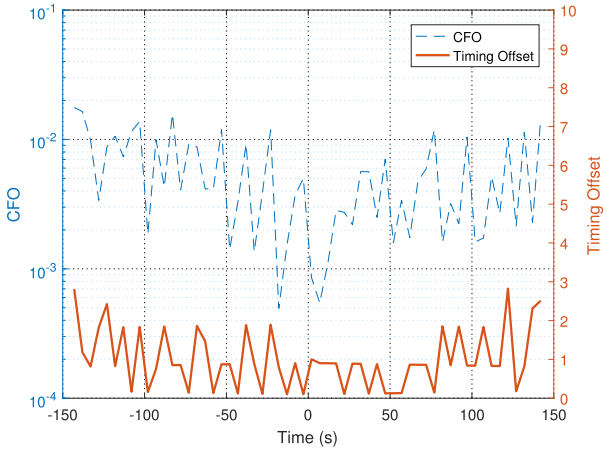

FIGURE 11. Estimation performance of the proposed algorithm in tracking synchronization in terms of the deviation between the estimated value and actual value over AWGN channel.

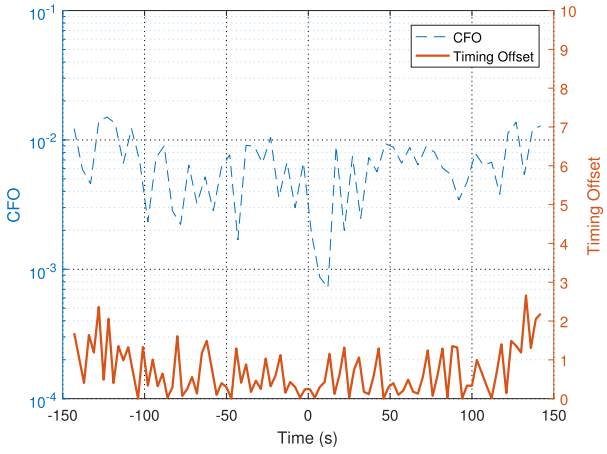

FIGURE 12. Estimation performance of the proposed algorithm in tracking synchronization in terms of the deviation between the estimated value and actual value over multipath fading channel.

In tracking synchronization, the parameters used to calculate the dynamic SNR are summarized in Table 4. In the visibility window, the performance of time-frequency tracking synchronization is shown in Fig.11 and Fig.12 in terms of the deviation between the estimated value and actual value. The tracking results show that the time tracking error can be limited to three sampling intervals, and the frequency tracking error can be limited to no more than 2% of the subcarrier spacing. Therefore, the achieved initial synchronization state can be maintained by the proposed algorithm in tracking synchronization during the overtopping procedure of satellite.

TABLE 4. Parameters used in downlink budget.

Parameter	Value	
Channel model	AWGN	Multipath
Carrier frequency	20GHz	3.5GHz
System bandwidth	480MHz	20MHz
L_{other}	2dB	0dB
G/T ratio	2.6dB/K	-27.6dB/K
EIRP	35dBW	
Boltzmann constant	-228.6dBW/K/Hz	
Orbital altitude	600km	

VI. CONCLUSION

In this paper, we have investigated the downlink transmission for 5G integrated LEO mobile SatCom system, and proposed two algorithms for timing and frequency offset estimation applied for the synchronization signals of 5G NR in initial synchronization. The PSS scheme is exploiting the PSS alone where the estimate of timing and frequency offsets has been transformed into two one-dimensional search optimization problems. To further reduce the processing complexity of timing offset estimation, the involved higher dimensional matrix has been decomposed by the modulated DPSS vectors. The CP assistant scheme is utilizing both the structure of CP in multiple OFDM symbols and PSS, which further improve the estimation performance. Meanwhile, to avoid the frequency one-dimensional exhaustive search in the CP assistant scheme, a low-complexity method using the proposed PSS scheme based on the estimated FFO was also given. In addition, we proposed an estimation algorithm to track the change of the parameters including timing and frequency offset. The simulation results illustrated that the proposed algorithms are effective and feasible schemes to realize the accurate downlink time and frequency synchronization in typical SatCom systems.

Note that in this paper we omit oscillator frequency error between the satellite and the UE. The current work can be extended to such scenarios in the future work.

APPENDIX
PROOF OF THEOREM 1

Note that the equation (14) can be rewritten as

$$\begin{aligned}\log f\left(\mathbf{r}_0|\theta\right) &= \log f\left(\mathbf{r}_0|\theta,\varepsilon,\mathbf{h}\right) - \log\frac{f\left(\varepsilon,\mathbf{h}|\mathbf{r}_0,\theta\right)}{f\left(\varepsilon,\mathbf{h}|\theta\right)} \\ &= \int \log f\left(\mathbf{r}_0|\theta,\varepsilon,\mathbf{h}\right) f\left(\varepsilon,\mathbf{h}|\mathbf{r}_0,\theta\right) d\varepsilon d\mathbf{h} \\ &\quad + \int f\left(\varepsilon,\mathbf{h}|\mathbf{r}_0,\theta\right) \log\frac{f(\varepsilon,\mathbf{h})}{f\left(\varepsilon,\mathbf{h}|\mathbf{r}_0,\theta\right)} d\varepsilon d\mathbf{h}\end{aligned} \tag{59}$$

For convenience, we define

$$D_{KL}(f(\varepsilon,\mathbf{h}|\mathbf{r}_0,\theta),f(\varepsilon,\mathbf{h})) = \int f(\varepsilon,\mathbf{h}|\mathbf{r}_0,\theta)\log\frac{f(\varepsilon,\mathbf{h}|\mathbf{r}_0,\theta)}{f(\varepsilon,\mathbf{h})}d\varepsilon d\mathbf{h}. \quad (60)$$

Then, since $D_{KL}(f(\varepsilon,\mathbf{h}|\mathbf{r}_0,\theta),f(\varepsilon,\mathbf{h}))$ is the Kullback-Leibler (KL) divergence between $f(\varepsilon,\mathbf{h}|\mathbf{r}_0,\theta)$ and $f(\varepsilon,\mathbf{h})$, we have it is greater than zero. With the definition in (60) we obtain

$$\begin{aligned}\log f(\mathbf{r}_0|\theta) &= \int \log f(\mathbf{r}_0|\theta,\varepsilon,\mathbf{h}) f(\varepsilon,\mathbf{h}|\mathbf{r}_0,\theta)\,d\varepsilon d\mathbf{h} \\ &\quad - D_{KL}(f(\varepsilon,\mathbf{h}|\mathbf{r}_0,\theta),f(\varepsilon,\mathbf{h})) \\ &\geq \int \log f(\mathbf{r}_0|\theta,\varepsilon,\mathbf{h}) f(\varepsilon,\mathbf{h}|\mathbf{r}_0,\theta)\,d\varepsilon d\mathbf{h}\end{aligned}$$

Here Theorem 1 is proved.

REFERENCES

[1] F. Bastia, C. Bersani, E. A. Candreva, S. Cioni, G. E. Corazza, M. Neri, C. Palestini, M. Papaleo, S. Rosati, and A. Vanelli-Coralli, "LTE adaptation for mobile broadband satellite networks," *EURASIP J. Wireless Commun. Netw.*, vol. 2009, Nov. 2009, Art. no. 989062.

[2] M. Casoni, C. A. Grazia, M. Klapez, N. Patriciello, A. Amditis, and E. Sdongos, "Integration of satellite and LTE for disaster recovery," *IEEE Commun. Mag.*, vol. 53, no. 3, pp. 47–53, Mar. 2015.

[3] A. Guidotti, A. Vanelli-Coralli, M. Caus, J. Bas, G. Colavolpe, T. Foggi, S. Cioni, A. Modenini, and D. Tarchi, "Satellite-enabled LTE systems in LEO constellations," in *Proc. IEEE ICC*, Paris, France, May 2017, pp. 876–881.

[4] Y. Ruan, Y. Li, C.-X. Wang, and R. Zhang, "Energy efficient adaptive transmissions in integrated satellite-terrestrial networks with SER constraints," *IEEE Trans. Wireless Commun.*, vol. 17, no. 1, pp. 210–222, Jan. 2018.

[5] A. Guidotti, A. Vanelli-Coralli, M. Conti, S. Andrenacci, S. Chatzinotas, N. Maturo, B. Evans, A. Awoseyila, A. Ugolini, T. Foggi, L. Gaudio, N. Alagha, and S. Cioni, "Architectures and key technical challenges for 5G systems incorporating satellites," *IEEE Trans. Veh. Technol.*, vol. 68, no. 3, pp. 2624–2639, Mar. 2019.

[6] G. Giambene, S. Kota, and P. Pillai, "Satellite-5G integration: A network perspective," *IEEE Netw.*, vol. 32, no. 5, pp. 25–31, Sep./Oct. 2018.

[7] O. Kodheli, A. Guidotti, and A. Vanelli-Coralli, "Integration of satellites in 5G through LEO constellations," in *Proc. IEEE Global Commun. Conf. (GLOBECOM)*, Dec. 2017, pp. 1–6.

[8] A. Guidotti, A. Vanelli-Coralli, O. Kodheli, G. Colavolpe, and T. Foggi, "Integration of 5G technologies in LEO mega-constellations," *CoRR*, vol. 2, no. 1, Sep. 2017. [Online]. Available: https://arxiv.org/abs/1709.05807

[9] *Technical Specification Group Radio Access Network; Study on New Radio (NR) to Support Non Terrestrial Networks (Release 15)*, document TR 38.811, 3GPP, Aug. 2018.

[10] P. H. Moose, "A technique for orthogonal frequency division multiplexing frequency offset correction," *IEEE Trans. Commun.*, vol. 42, no. 10, pp. 2908–2914, Oct. 1994.

[11] Y. Mostofi and D. C. Cox, "Mathematical analysis of the impact of timing synchronization errors on the performance of an OFDM system," *IEEE Trans. Commun.*, vol. 54, no. 2, pp. 226–230, Feb. 2006.

[12] *Technical Specification Group Radio Access Network; NR; Physical Layer Procedures for Control (Release 15)*, document TS 38.213, 3GPP, Sep. 2018.

[13] I. Ali, N. Al-Dhahir, and J. E. Hershey, "Doppler characterization for LEO satellites," *IEEE Trans. Commun.*, vol. 46, no. 3, pp. 309–313, Mar. 1998.

[14] S. Amiri and M. Mehdipour, "Accurate Doppler frequency shift estimation for any satellite orbit," in *Proc. RAST*, Istanbul, Turkey, Jun. 2007, pp. 602–607.

[15] T. M. Schmidl and D. C. Cox, "Robust frequency and timing synchronization for OFDM," *IEEE Trans. Commun.*, vol. 45, no. 12, pp. 1613–1621, Dec. 1997.

[16] H. Minn, M. Zeng, and V. K. Bhargava, "On timing offset estimation for OFDM systems," *IEEE Commun. Lett.*, vol. 4, no. 7, pp. 242–244, Jul. 2000.

[17] H. Minn, V. K. Bhargava, and K. B. Letaief, "A robust timing and frequency synchronization for OFDM systems," *IEEE Trans. Wireless Commun.*, vol. 2, no. 4, pp. 822–839, Jul. 2003.

[18] H.-T. Hsieh and W.-R. Wu, "Maximum likelihood timing and carrier frequency offset estimation for OFDM systems with periodic preambles," *IEEE Trans. Veh. Technol.*, vol. 58, no. 8, pp. 4224–4237, Oct. 2009.

[19] M. Sandell, J. V. D. Beek, and P. O. Börjesson, "Timing and frequency synchronization in OFDM systems using the cyclic prefix," in *Proc. Int. Symp. Synchronization*, Essen, Germany, Dec. 1995, pp. 16–19.

[20] J.-J. van de Beek, M. Sandell, and P. O. Borjesson, "ML estimation of time and frequency offset in OFDM systems," *IEEE Trans. Signal Process.*, vol. 45, no. 7, pp. 1800–1805, Jul. 1997.

[21] M.-H. Hsieh and C.-H. Wei, "A low-complexity frame synchronization and frequency offset compensation scheme for OFDM systems over fading channels," *IEEE Trans. Veh. Technol.*, vol. 48, no. 5, pp. 1596–1609, Sep. 1999.

[22] V. Krishnamurthy, C. R. N. Athaudage, and D. Huang, "Adaptive OFDM synchronization algorithms based on discrete stochastic approximation," *IEEE Trans. Signal Process.*, vol. 53, no. 4, pp. 1561–1574, Apr. 2005.

[23] T. Fusco and M. Tanda, "Blind synchronization for OFDM systems in multipath channels," *IEEE Trans. Wireless Commun.*, vol. 8, no. 3, pp. 1340–1348, Mar. 2009.

[24] W.-L. Chin, C.-W. Kao, H.-H. Chen, and T.-L. Liao, "Iterative synchronization-assisted detection of OFDM signals in cognitive radio systems," *IEEE Trans. Veh. Technol.*, vol. 63, no. 4, pp. 1633–1644, May 2014.

[25] Y. Kang, S. Kim, D. Ahn, and H. Lee, "Timing estimation for OFDM systems by using a correlation sequence of preamble," *IEEE Trans. Consum. Electron.*, vol. 54, no. 4, pp. 1600–1608, Nov. 2008.

[26] Y. Liu, T. F. Wong, and A. Pandharipande, "Timing estimation in multiple-antenna systems over Rayleigh flat-fading channels," *IEEE Trans. Signal Process.*, vol. 53, no. 6, pp. 2074–2088, Jun. 2005.

[27] Z. Zhang, J. Liu, and K. Long, "Low-complexity cell search with fast PSS identification in LTE," *IEEE Trans. Veh. Technol.*, vol. 61, no. 4, pp. 1719–1729, May 2012.

[28] M. Morelli and M. Moretti, "A robust maximum likelihood scheme for PSS detection and integer frequency offset recovery in LTE systems," *IEEE Trans. Wireless Commun.*, vol. 15, no. 2, pp. 1353–1363, Feb. 2016.

[29] M. H. Nassralla, M. M. Mansour, and L. M. A. Jalloul, "A low-complexity detection algorithm for the primary synchronization signal in LTE," *IEEE Trans. Veh. Technol.*, vol. 65, no. 10, pp. 8751–8757, Oct. 2016.

[30] W. Xu and K. Manolakis, "Robust synchronization for 3GPP LTE system," in *Proc. IEEE GLOBECOM*, Miami, FL, USA, Dec. 2010, pp. 1–5.

[31] H. Abdzadeh-Ziabari and M. G. Shayesteh, "Robust timing and frequency synchronization for OFDM systems," *IEEE Trans. Veh. Technol.*, vol. 60, no. 8, pp. 3646–3656, Oct. 2011.

[32] *Technical Specification Group Radio Access Network; NR; Physical Channels and Modulation (Release 15)*, document TS 38.211, 3GPP, Sep. 2018.

[33] H.-J. Zepernick and A. Finger, *Pseudo Random Signal Processing: Theory Application*. Hoboken, NJ, USA: Wiley, 2013.

[34] M. A. Davenport and M. B. Wakin, "Compressive sensing of analog signals using discrete prolate spheroidal sequences," *Appl. Comput. Harmon. Anal.*, vol. 33, no. 3, pp. 438–472, Nov. 2012.

[35] D. Slepian, "Prolate spheroidal wave functions, Fourier analysis, and uncertainty—V: The discrete case," *Bell Syst. Tech. J*, vol. 57, no. 5, pp. 1371–1430, May/Jun. 1978.

WENJIN WANG (M'14) received the Ph.D. degree in communication and information systems from Southeast University, Nanjing, China, in 2011. From 2010 to 2014, he was with the School of System Engineering, University of Reading, Reading, U.K. He is currently an Associate Professor with the National Mobile Communications Research Laboratory, Southeast University, Nanjing. His research interests include advanced signal processing for future wireless communications and satellite communications. He was a recipient of the Best Paper Award at IEEE WCSP 2009 and the first grade Technological Invention Award of the State Education Ministry of China, in 2009.

YUSHAN TONG received the B.E. and M.E. degrees in information engineering from Southeast University, Nanjing, China, in 2016 and 2019, respectively, where he was with the National Mobile Communications Research Laboratory. He is currently an Engineer with Huawei Technologies Company Ltd., Shanghai, China. His research interest includes satellite communications.

LINGXUAN LI received the B.E. degree in information engineering from Southeast University, Nanjing, China, in 2018. She is currently pursuing the M.E. degree with the National Mobile Communications Research Laboratory. Her research interests include communications and hardware implementation, with emphasis on satellite communications.

AN-AN LU (S'11–M'17) received the B.E., M.E., and Ph.D. degrees in electronic engineering from Southeast University, Nanjing, China, in 2006, 2012, and 2017, respectively. From 2006 to 2008, he was with the Research Department, Hejian Technology Company Ltd., Suzhou, China. From 2014 to 2016, he visited the Missouri University of Science and Technology, Rolla, MO, USA. He is currently a Lecturer with the National Mobile Communications Research Laboratory, Southeast University. His research interests include information theory and wireless communications.

LI YOU (S'13–M'17) received the B.E. and M.E. degrees in electrical engineering from the Nanjing University of Aeronautics and Astronautics, Nanjing, China, in 2009 and 2012, respectively, and the Ph.D. degree in electrical engineering from Southeast University, Nanjing, China, in 2016.

From 2014 to 2015, he conducted visiting research with the Center for Pervasive Communications and Computing, University of California at Irvine, Irvine, CA, USA. Since 2016, he has been with the Faculty of the National Mobile Communications Research Laboratory, Southeast University. His research interests include communications, signal processing, and information theory, with current emphasis on massive MIMO communications.

XIQI GAO (S'92–AM'96–M'02–SM'07–F'15) received the Ph.D. degree in electrical engineering from Southeast University, Nanjing, China, in 1997.

He joined the Department of Radio Engineering, Southeast University, in 1992. From 1999 to 2000, he was a Visiting Scholar with the Massachusetts Institute of Technology, Cambridge, MA, USA, and Boston University, Boston, MA, USA. Since 2001, he has been a Professor of information systems and communications. From 2007 to 2008, he visited the Darmstadt University of Technology, Darmstadt, Germany, as a Humboldt Scholar. His current research interests include broadband multicarrier communications, MIMO wireless communications, channel estimation and turbo equalization, and multirate signal processing for wireless communications.

Dr. Gao received the Science and Technology Awards of the State Education Ministry of China, in 1998, 2006, and 2009, the National Technological Invention Award of China, in 2011, and the 2011 IEEE Communications Society Stephen O. Rice Prize Paper Award in the field of communications theory. He served as an Editor for the IEEE TRANSACTIONS ON WIRELESS COMMUNICATIONS, from 2007 to 2012 and the IEEE TRANSACTIONS ON SIGNAL PROCESSING, from 2009 to 2013. He currently serves as an Editor for the IEEE TRANSACTIONS ON COMMUNICATIONS.